Available online at www.sciencedirect.com
ScienceDirect
Sensors and Actuators A 139 (2007) 194–202
SENSORS AND ACTUATORS A PHYSICAL
www.elsevier.com/locate/sna

A novel electromagnetic elastomer membrane actuator with a semi-embedded coil

Hung-Lin Yin [a], Yu-Che Huang [b], Weileun Fang [b], Jerwei Hsieh [a,*]

[a] Instrument Technology Research Center (ITRC), National Applied Research Laboratories (NARL), 20 R&D Road VI, Hsinchu Science-based Industrial Park, Hsinchu 300, Taiwan, ROC
[b] Department of Power Mechanical Engineering, National Tsing Hua University, 101, Section 2 Kuang Fu Road, Hsinchu, 300, Taiwan, ROC

Received 31 July 2006; received in revised form 19 December 2006; accepted 4 January 2007
Available online 12 January 2007

Abstract

This study describes the design, fabrication, and testing of a novel electromagnetic membrane actuator (EMMA) for pumping applications. Related technologies for realizing membrane micropump are first reviewed. A conceptual design and batch process for fabricating thin PDMS membrane embedded with a planar coil, which is the essential part of EMMA, is then proposed. This study investigates some important issues relating to the utilization of PDMS in pneumatic pumping. An advanced EMMA with improved fabrication yield and reliability is also presented. To demonstrate the feasibility, different types of EMMA are fabricated and tested. The EMMA with membrane diameter of 7 mm was tested, and a deflection exceeding 50 μm can be achieved with an applied current of less than 500 mA. Stability and reliability tests also showed promising results. To summarize, the proposed EMMA can fulfill the requirements of large flexibility, good controllability, system compactness and batch-process capability, and can be used to establish a simple and effective pumping system.
© 2007 Elsevier B.V. All rights reserved.

Keywords: Electromagnetic; Membrane; Micropump; Planar coil; PDMS

1. Introduction

Microfluidic devices for biomedical analysis system potentially possess many advantages, such as portability, low sample/reagent volume, high sensitivity and low cost [1]. As essential components in microfluidic devices, micropumps are extremely important and have been studied extensively [2]. Various actuation principles have been employed in micropumps [3–9], and membrane type actuators are commonly exploited in such applications. Numerous materials have been used as the actuator membranes of micropumps, including silicon [10], metal [11], low stress nitride [12], parylene [13], polyimide [14], silicon rubber [15] and PDMS [16]. Membranes made by silicon, metal and low-stress nitride are relatively stiff, and thus are limited to low-displacement applications. Parylene, polyimide, and silicon elastomer are biocompatible materials, and are commonly used in biomedical devices. However, the former two materials still possess larger stiffness than silicon elastomer. This work selected PDMS as the membrane material owing to its low stiffness and relative ease of processing. Certain other advantages, such as bio-compatibility, conformal contact to other surfaces, transparency, and low cost, are also beneficial in numerous applications.

Several actuation principles can be applied to actuate the PDMS membrane, including piezoelectric [3], electrostatic [4], thermopneumatic [5], electrochemical [6], shape memory alloy [7], magnetic [8], and electromagnetic [9]. In the case of piezoelectric and electrostatic actuation, high voltages of up to several hundred volts are generally required. Thermopneumatic and shape memory alloy actuators can more easily achieve larger displacements, while their response time is limited. Because of these limitations, electromagnetic actuators are more attractive due to their rapid response time, large deflection and relatively low power consumption. Both M. Khoo et al. [8] and C. Yamahata et al. [16] have demonstrated micro magnetic PDMS membrane actuators. Special treatment is required in their fabrication process, including electroplating of Permalloy and manual assembly of magnets into PDMS membrane.

* Corresponding author. Tel.: +886 3 5779911x337; fax: +886 3 5773947.
E-mail address: jerwei@itrc.org.tw (J. Hsieh).

0924-4247/$ – see front matter © 2007 Elsevier B.V. All rights reserved.
doi:10.1016/j.sna.2007.01.003

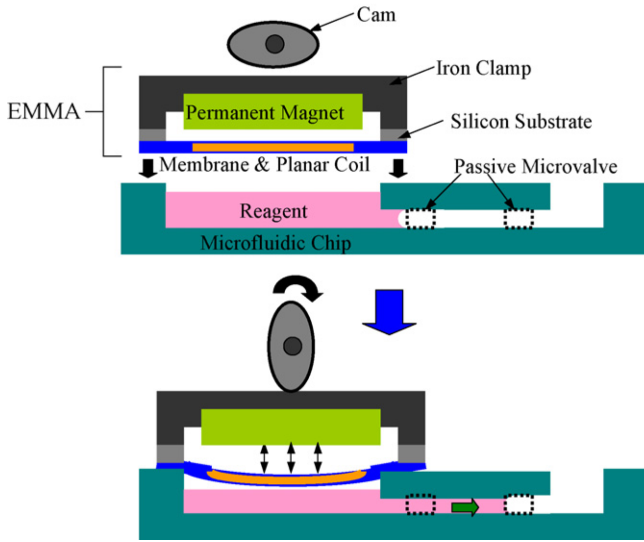

Fig. 1. Schematic illustration of a pumping apparatus utilizing EMMA.

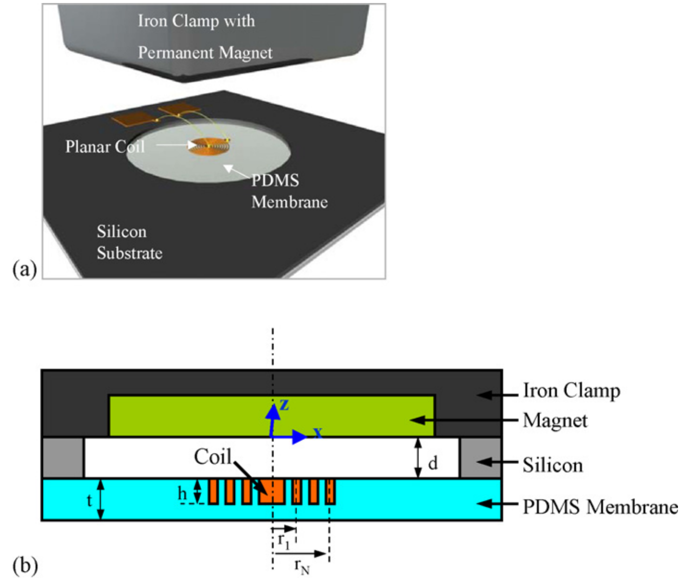

Fig. 2. Proposed EMMA module: (a) exploded view and (b) cross-section view.

Additionally, external magnets or electromagnets were required to control membrane movement.

This study proposes an electromagnetic membrane actuator (EMMA) that simultaneously fulfills the requirements of large flexibility, good controllability, system compactness and batch-process capability. PDMS serves as the membrane material, and a copper micro coil is embedded in the membrane to actively control its position. To further improve the actuator performance, a design for EMMA integrated with a semi-embedded electromagnetic coil is also proposed. Temporarily coupling EMMA with a microfluidic chip can construct a simple and effective pumping system, as shown in Fig. 1 [17]. Fluids in the microfluidic chip can be driven forward by a local pneumatic pressure provided by EMMA.

This study presents details related to the design and fabrication of EMMA. The advantages of integrating EMMA with a semi-embedded coil are also described. Additionally, important issues for utilizing PDMS in pneumatic pumping are investigated. To demonstrate the feasibility, different types of EMMA were fabricated using the proposed fabrication process. Static and dynamic testing of EMMA was performed, and the results are presented below.

2. Conceptual design for EMMA

2.1. Actuating principle

Fig. 2 schematically depicts the proposed EMMA. It basically consists of a permanent magnet, a PDMS membrane, and an embedded planar coil. Upon applying a current I to the coil, which has N turns, an electromagnetic field is generated. This field is interacted with that of a permanent magnet, and an electromagnetic force is produced as a result. To simplify the calculation of this force, the coil is modeled as a combination of many individual concentric coils [18]. Refer to Fig. 2(b), the electromagnetic force exerted on the i_{th} coil F_i, can be calculated as [19,20]:

$$F_i = I(\pi r_i^2)\frac{\partial B(z)}{\partial z} \quad (1)$$

where r_i denotes the radius of each individual coil, $B(z)$ represents the distribution of magnetic flux density of permanent magnet along z-axis, and d is the vertical distance between the center of the coil and that of the bottom surface of the magnet. For the radius of the movable membrane much larger than that of the coils, F_i can be approximated as applying at the center of the coil-embedded membrane. Assume a uniform field gradient of the permanent magnet. An effective concentrated force can thus be derived as:

$$F_{\text{eff}} = \sum_{i=1}^{N} F_i = \sum_{i=1}^{N} I(\pi r_i^2)\frac{\partial B(z)}{\partial z} \quad (2)$$

In applying the electromagnetic force to a pumping system, as shown in Fig. 1, it is imperative to know how much pressure the pumping system can provide and how much fluid volume it can drive. A demonstration system illustrated in Fig. 3 is used to estimate the quantities of interest. As the PDMS membrane fully covering a reservoir, the center deflection of the membrane

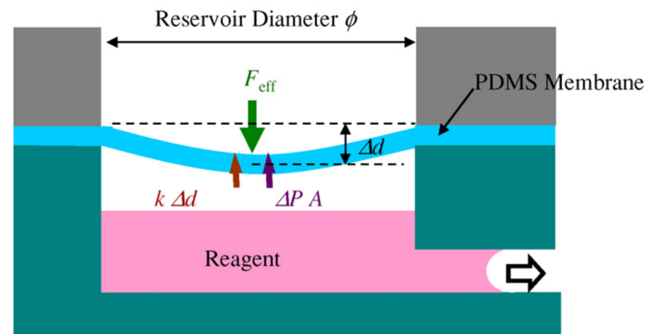

Fig. 3. Analytical model for pneumatic pumping application.

Δd can be derived as:

$$\Delta d = \frac{F_{\text{eff}} - \Delta PA}{k_{\text{eff}}} \quad (3)$$

where k_{eff} denotes the effective stiffness of the PDMS membrane with an embedded coil, ΔP represents the pneumatic pressure generated by the compression of air, and A is the surface area of the reservoir. The membrane can be regarded as a circular plate since its diameter is much larger than its thickness. For a central loading, the effective stiffness of a circular membrane with a fixed edge can be described as [21]:

$$k_{\text{eff}} = \frac{E_{\text{eff}} t^3}{0.00497 \times 12(1 - \upsilon^2)\phi^2} \quad (4)$$

where E_{eff} denotes the effective Young's Modulus of the PDMS membrane with an embedded coil, υ represents the Poisson ratio of the membrane, and t and ϕ are the membrane thickness and reservoir diameter, respectively. The pneumatic pressure ΔP generated by the volume change ΔV can be derived as:

$$\Delta P = \frac{V_0^{\gamma} - (V_0 - \Delta V)^{\gamma}}{(V_0 - \Delta V)^{\gamma}} P_0 \quad (5)$$

where P_0 denotes the atmospheric pressure, V_0 represents the original volume of the sealing air, and γ is the adiabatic coefficient of 1.4 for air. In Eq. (5), the effect of heat transformation is ignored and the adiabatic condition is adopted [22]. For a fixed-edge boundary condition, a center deflection Δd leads to a volume change ΔV given by:

$$\Delta V = \int_0^{\phi/2} \int_0^{2\pi} \Delta d \left[1 - \cos\frac{2\pi r \cos\theta}{\phi}\right] \times \left[1 - \cos\frac{2\pi r \sin\theta}{\phi}\right] \mathrm{d}r\, \mathrm{d}\theta \quad (6)$$

Substituting Eqs. (2), (4), (5) and (6) into Eq. (3), the pneumatic pressure under different applying currents of I can be obtained. It is noted that for the cases where the electromagnetic force cannot be approximated as a concentrated force, this operation will overestimate the membrane deflection as well as the generated pneumatic pressure.

In this work, an NdFeB permanent magnet assembled in an iron clamp is exploited to provide the magnetic field. Using a Gaussmeter, the distribution of $B(z)$ is measured and curve-fitted as:

$$B(z) = 0.4658 - 239.9z + 50828z^2 - 5 \times 10^6 z^3 + 2 \times 10^8 z^4 (T) \quad (7)$$

Substituting Eq. (7) into Eq. (1), F_i can be derived. The numerical calculation results show that typical electromagnetic force is in the range of tens to hundreds μN, membrane deformation reaches up to several tens of micrometers, and the pneumatic pressure can reach several kPa by applying a current I of less than 500 mA. Although Eqs. (1) and (2) reveals that larger coil radius r_i and coil number N can result in larger electromagnetic force, the effective Young's Modulus E_{eff} as well as the effective stiffness k_{eff} would also increase. As a result, there would be an optimal coil design for generating the largest membrane deflection.

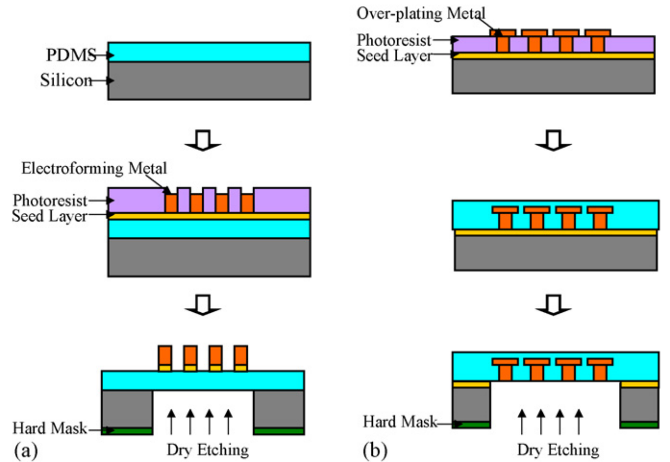

Fig. 4. The process with (a) a standard lithography and an electroforming (b) an over-plating technique for the EMMA.

2.2. EMMA integrated with a semi-embedded coil

In realizing the EMMA, a conducting coil integrated with a PDMS membrane is required. Fig. 4(a) shows a straightforward process for realizing the EMMA. However, it is difficult to perform a standard lithography on top of PDMS membrane because of its high thermal expansion coefficient and hydrophobic surface. Additionally, the metal patterns would peel from the membrane surface during operation. Accordingly, an electroforming metal with over-plating technique is used to overcome this difficulty. The copper line is over-plated to form a mushroom shape, as shown in Fig. 4(b). The PDMS is then spun on the substrate to fully cover the copper line with a definite thickness. The metal line with mushroom shape automatically forms an embedded mechanism with the PDMS membrane. Consequently, a firm coil-membrane composite can then be realized.

Despite the advantages mentioned above, the embedded metal coil (as shown in Fig. 5(a)) increases the effective stiffness of PDMS membrane, and thus significantly limits deflection. Reducing the thickness of the coil can decrease overall stiffness,

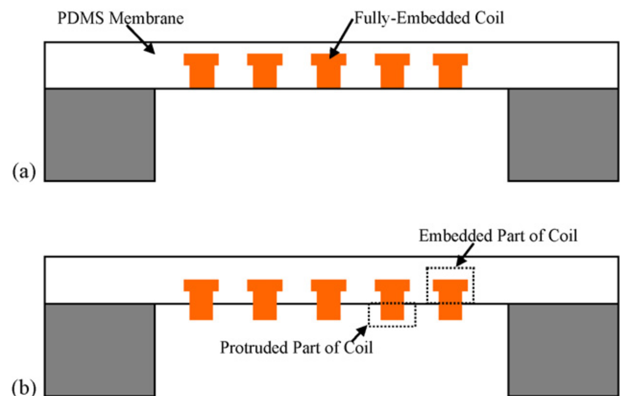

Fig. 5. The EMMA with (a) a fully-embedded coil and (b) a semi-embedded coil.

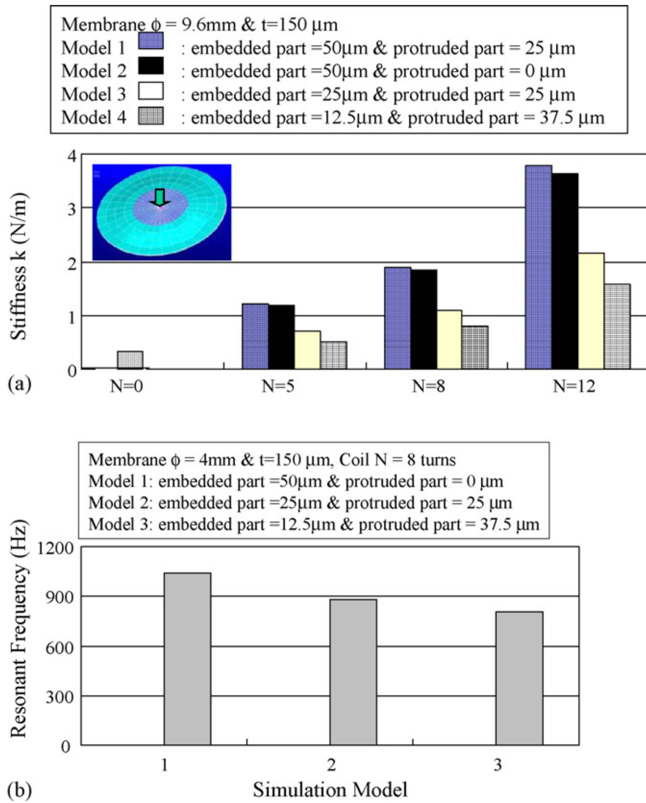

Fig. 6. Simulation result of (a) effective stiffness and (b) resonance frequency.

but also increases the consuming power due to the increased resistance. As applying a current I on a coil, the relationship between the consuming power P and the cross-section area A of the coil is described as:

$$P \propto A^{-1} \tag{8}$$

To further improve performance, this study also proposes an advanced EMMA. The highlight of this design is a semi-embedded coil with a protruded part, as shown in Fig. 5(b). The protruded part of the coil, which can essentially be considered a free-standing structure, contributes only slightly to the composite membrane stiffness. Meanwhile, the protruded part can provide an extra cross-section area of the coil, which would significantly decrease the resistance. According to Eq. (8), the consuming power can be reduced and a good stability of EMMA can also be expected due to the reduction of joule heating.

To confirm the effectiveness of the proposed EMMA, the behavior of PDMS membrane with a semi-embedded coil was analyzed using an FEM simulation tool (ANSYS 10.0). The coil thickness is set the same in different simulation models, while the percentage of the embedded depth is varied. By comparing Model 1 with Model 2 in Fig. 6(a), the deviations of stiffness are within 2% while the protruded part of the coil increases and the embedded part remain unchanged. As expected, the effective stiffness only slightly changed with the dimension of the protruded part of the coil. Since the cross-section area of the coil remains the same, the consuming power remains unaffected. On the other hand, different resonant frequency of the EMMA can also be derived without altering the mask layout of the coil. By adjusting the percentage of the protruded part, the first resonant frequency of the EMMA can be set to range between 1.04 kHz and 0.8 kHz, as illustrated in Fig. 6(b).

2.3. Fabrication process for the advanced EMMA

Fig. 7 shows the process for fabricating EMMA with a semi-embedded coil. First, extending trenches are formed by dry etching of silicon substrate, as shown in Fig. 7(a). These trenches can create external spaces for electroforming the specific shape of the proposed semi-embedded coils. Furthermore, it has the advantage of improving the aspect ratio for the electroformed structure. Second, an ICP-SCREAM technology [23] is performed to made mechanical interlocking trenches to improve PDMS adhesion, as shown in Fig. 7(b). Section 3.3 will present the relevant details. Subsequently, a SiO_2 layer of 1 μm thickness is thermally grown, as shown in Fig. 7(c). This material serves as a stop layer to protect the PDMS membrane against damage from dry etching. Following some lithography and electroforming steps, a copper coil with 50 μm thickness is fabricated, as shown in Fig. 7(d) and (e). The copper line is over-plated to form a mushroom shape as an interlocking structure. PDMS shown in Fig. 7(f) is then spin-coated and thermally treated to obtain a membrane thickness of roughly 127 μm. As shown in Fig. 7(g), the conducting pads are then formed on the backside of substrate using a lift-off technique. To release the membrane, an etching-through process is performed via silicon dry etching, as shown in Fig. 7(h). The dry etching process automatically stops at the SiO_2 layer, which is then removed by wet etching. Finally, an electronic path between conducting pads and the coil is formed through a wire-bonding process, as shown in Fig. 7(i).

Since all these fabrication steps can be performed without manual assembly or treatment, the proposed process is expected to achieve a reliable batch fabrication of the EMMA.

3. Characterization of PDMS membrane

PDMS is commonly used in passive structures such as microfluidic chips. To exploit PDMS in applications involving active actuators, some more properties must be taken into consideration. This work has studied some of the main issues, including the preparation of thin PDMS membrane, the resistance to etching process, adhesion improvement, and testing of the gas-permeation property of PDMS membrane. Details are presented in the following sections.

3.1. Preparation of thin PDMS membrane

A thin PDMS film with thickness ranging from tens to hundreds of micrometers is required for the application of EMMA. This study utilizes spin-coating to achieve such a thin film. Before coating, the Sylgard 184 PDMS (from Dow Corning Co.) was mixed with a curing agent and placed in a vacuum chamber for degassing. Following pouring and spinning, thermal treatment was performed at 100 °C for an hour. Based on the thickness measurement results shown in Fig. 8, different degassing times are shown to result in slightly different thick-

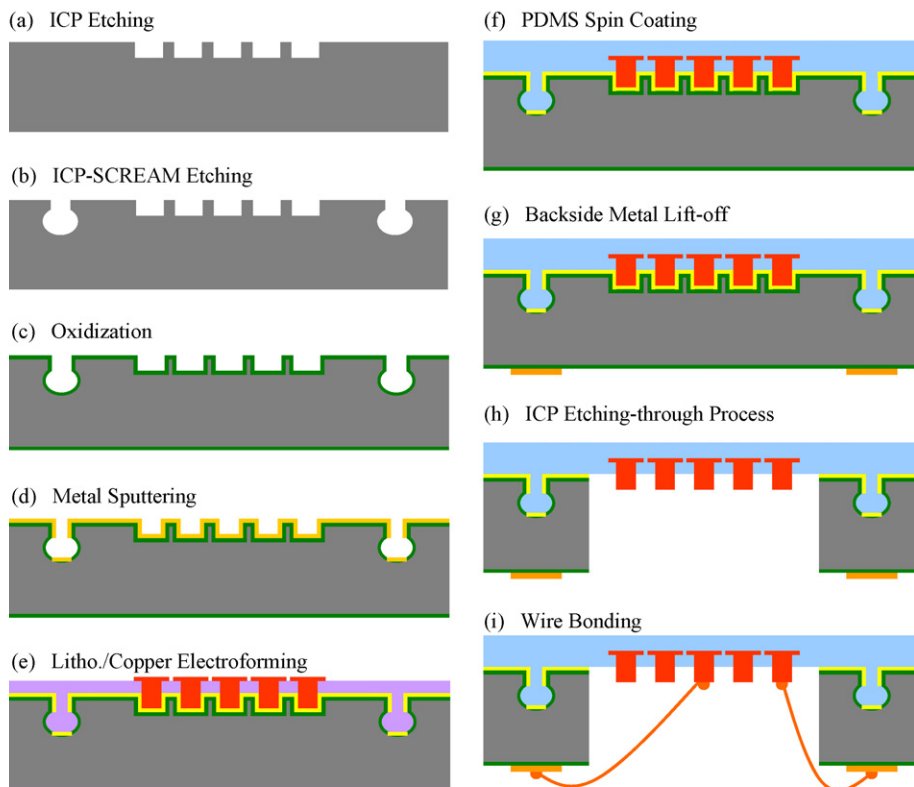

Fig. 7. Fabrication process of EMMA with a semi-embedded coil.

ness. Typical thicknesses are in the range of 20–144 μm. Double spin coating can achieve maximum thickness up to 479 μm. Tests for the uniformity of PDMS thin film demonstrated a 144 μm-thick PDMS with ±1.4% of thickness variation for a 500 rpm single spin on a 4 inch wafer.

3.2. Resistance to different etching processes

Designing the fabrication process for the PDMS membrane requires knowing its resistance to different etching processes. Chemical resistance was performed by measuring the weight loss of a PDMS piece after immersing it into the chemical etching solution for 30 min. A precision balance with 0.5 mg resolution was used to measure the weight change of the PDMS piece. The test result revealed that except for HF, PDMS has good chemical resistance to most etching solutions commonly used in MEMS fabrication, including BOE, KOH, and etching solutions for metals. Energy dispersive spectrometer (EDS) analysis indicated that the percentage of atomic weight is slightly changed after HF etching. This study also examined the plasma damage of PDMS during dry etching. Cracks in the PDMS surface were clearly observed even when the applied power of the bottom electrode was set below 10 mW. A stronger ion-bombarded effect during silicon dry etching is expected due to a larger applied power (>12 mW) and the addition of Ar^+ ions. As a result, a protective layer is required to prevent the PDMS surface from plasma damage during dry etching.

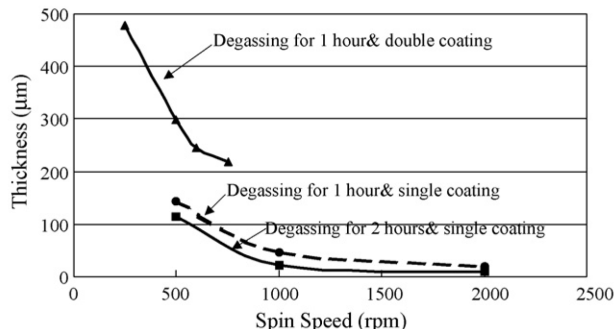

Fig. 8. Diagram of spin speed vs. PDMS thickness.

3.3. Adhesion improvement

To serve as an EMMA, the adhesion between PDMS membrane and the substrate surface strongly influences device lifetime. To understand the adhesion force of different interfaces, PDMS films coated on various surfaces, including single crystal silicon (SCS), poly-silicon, SiO_2, Si_3N_4, Cr/Au, and Ti/Cu, were prepared. Each sample was subjected to scratch test using a nanoindentor. The testing result displayed in Fig. 9 demonstrates that the critical load, which corresponds to the adhesion force, can be improved using an appropriate interface material. For example, the adhesion between PDMS and SCS, which has a critical load of 28 mN, could be enhanced by adding a SiO_2 layer to achieve a critical load of 32 mN. Moreover, the critical load between PDMS and poly-silicon (=53 mN) was twice that between PDMS and SCS, owing to its rougher surface.

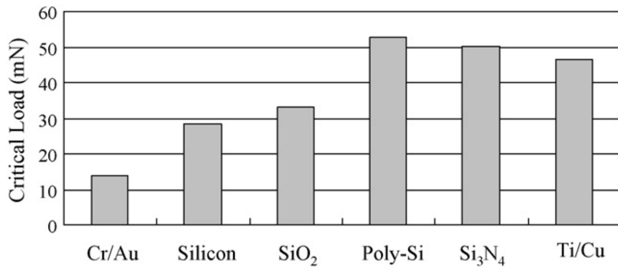

Fig. 9. Scratch testing of PDMS film on various surfaces.

Although adding an interface layer can somewhat improve PDMS adhesion, it may be inadequate for high yield fabrication. For example, if the surface to be processed is not clean enough, the PDMS membrane may still peel form that surface even with the presence of a SiO_2 interface layer, as shown in Fig. 10. Accordingly, a fabrication method for forming a mechanical interlocking is proposed to further improve adhesion. As shown in Fig. 11(a), the ICP-SCREAM technology was used to fabricate "reversed T-shaped" trenches. After spin coating, the PDMS filled into the trenches and automatically formed mechanical interlocking. As shown in Fig. 11(b), mechanical interlocking with a complementary shape to the T-shaped silicon trench is clearly observable. The proposed method significantly improved the process yield.

3.4. Gas-permeation property of PDMS

For an EMMA applied in the pneumatic-pumping application, the gas-permeation property of PDMS film must be considered. To investigate this phenomenon, an experiment to test for gas-permeation was carried out, the setup of which is shown in Fig. 12(a). The water levels at both ends of a U-shaped tube, one end of which was sealed with a PDMS film, were recorded over a period of time. The difference between the two levels can be converted into the pressure loss caused by gas-permeation of the PDMS film. Fig. 12(b) shows the measured pressure loss for a PDMS film with 127 μm thickness. The figure reveals that for a sealing air with pressure of $P = 5$ kPa, the pressure change measured after 24 h can be lower than 0.06 kPa, corresponding to a 1% pressure loss. Thus despite being gas-permeable, PDMS remains adequate as a membrane material for pneumatic-pumping application.

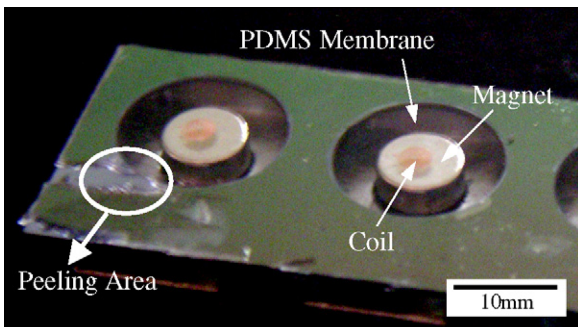

Fig. 10. Photo of PDMS membrane peeling from a SiO_2 layer.

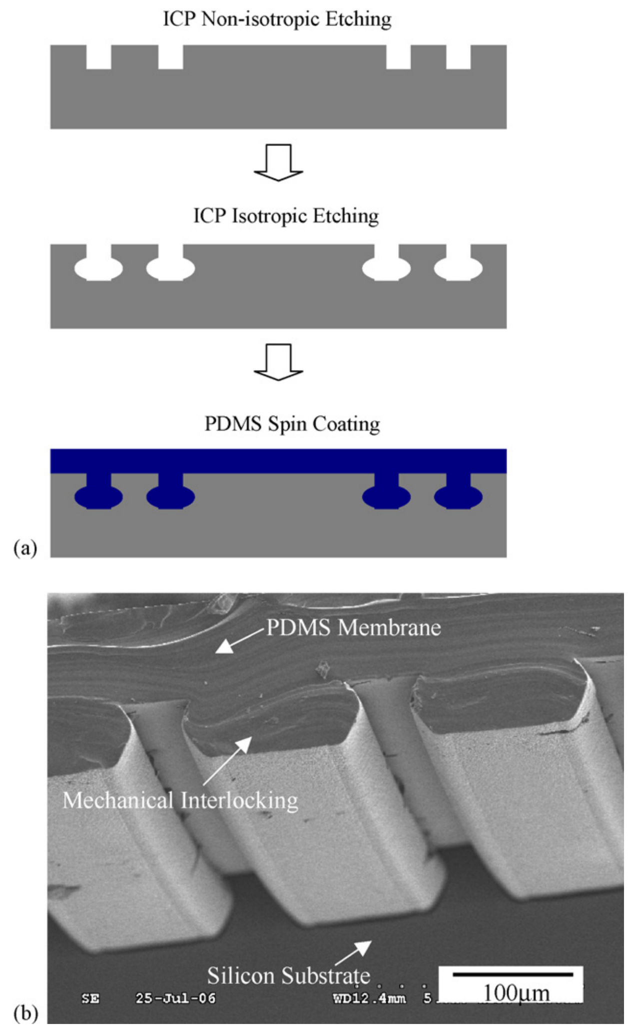

Fig. 11. (a) Fabrication process of SCREAM technology. (b) SEM picture of PDMS. mechanical interlocking.

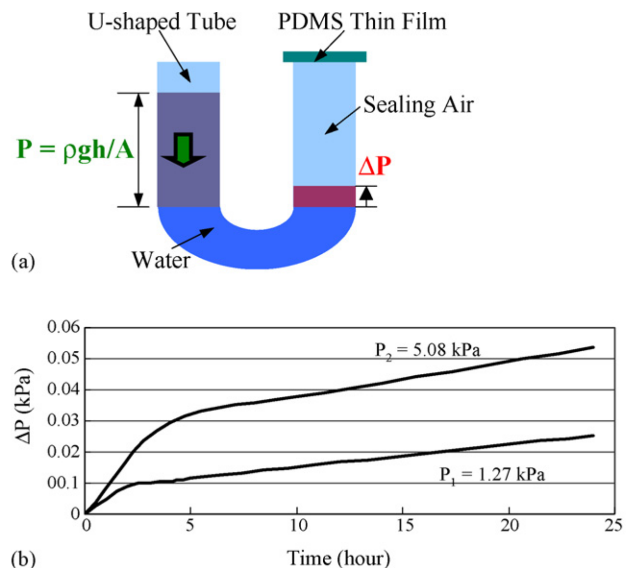

Fig. 12. (a) Experimental setup for gas-permeation test. (b) Diagram of experimental result.

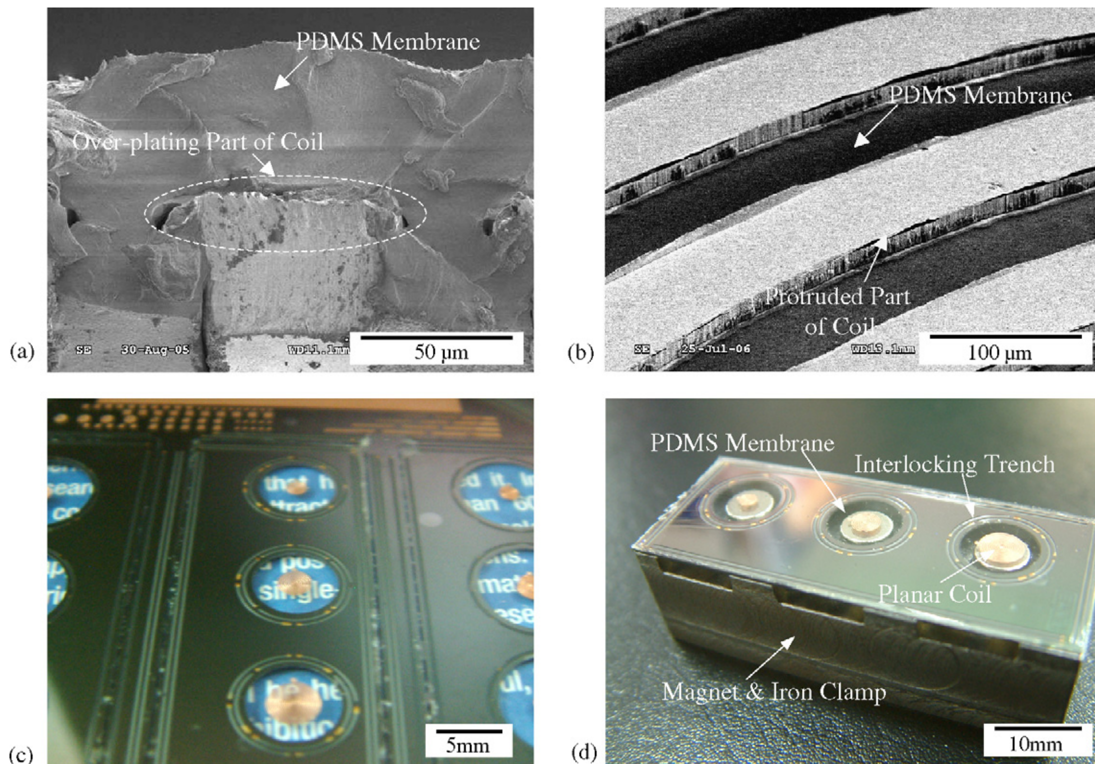

Fig. 13. Fabrication results: (a) SEM picture of PDMS membrane with an over-plating embedded coil, (b) backside view of PDMS membrane with a semi-embedded coil, (c) photo of EMMA chip and (d) photo of EMMA module.

4. Characterization for EMMA

4.1. Fabrication results

Fig. 13 shows some fabrication results of EMMAs with semi-embedded coils. The cross-sectional view of the SEM picture shows that the PDMS membrane with an embedded copper coil was successfully fabricated. The copper coil could remain in the PDMS membrane without position shifting or peeling when the membrane was deformed. The SEM picture shown in Fig. 13 (b) reveals a promising result from fabricating the semi-embedded coil with a protruded part. The fabricated PDMS membrane has such good flatness that the characters behind the membrane are clearly visible without distortion, as illustrated in Fig. 13(c). The measured central deformation of a membrane with $\phi = 4$ mm is below 10 μm. By using mechanical interlocking to enhance the adhesion, the PDMS membrane surrounded by mechanical interlocking could attach to the silicon substrate without any peeling, as shown in Fig. 13(d). The process yield was significantly improved with this approach. The figure also shows an entire EMMA module, including a chip of the PDMS membrane with a semi-embedded copper coil, an NdFeB magnet, and an iron clamp.

4.2. Driving testing of EMMA

To perform the static driving testing, a microscope with 0.5 μm z-axis resolution was used to measure the quasi-static displacement of the membrane. The 7 mm-diameter EMMAs with different turns of coils N were tested. The results shown in Fig. 14 reveal that by applying current of 500 mA, the maximum displacement at the center of the PDMS membrane can reach 55 μm, equivalent to a pumping volume exceeding 2 μl. This measured displacement is about 5–6-fold smaller comparing with that computed from the theory of Section 2.1. Since the device-under-test contains coils with max. diameter around 4 mm, which is comparable with that of the movable membrane, the mismatch is as expected. Inaccurate material parameters may also contribute to this result. Measurement results also reveal that the maximum dissipated power is around 0.5 W and the temperature raises to 110 °C for an applying current of 500 mA. Stability testing was also performed, the results of

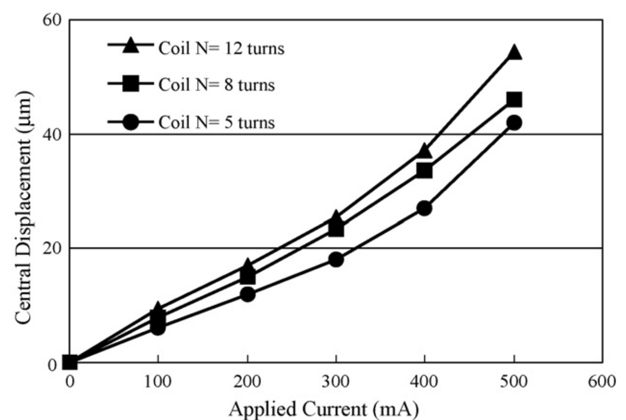

Fig. 14. Experimental result of static deflection.

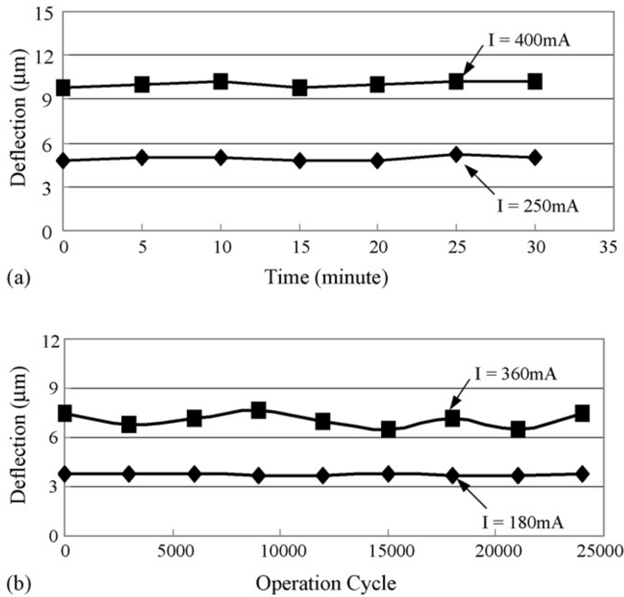

Fig. 15. Experimental result of (a) stability testing and (b) reliability testing.

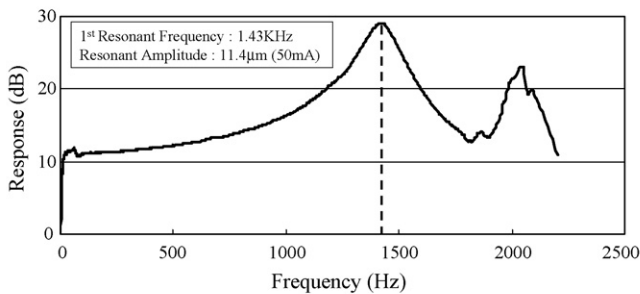

Fig. 16. Experimental result of dynamic testing.

which are shown in Fig. 15(a). For a 4 mm-diameter EMMA with an eight turns coil, no obvious deflection deviation was observable in a 30 min testing, sufficient long for processing a full chemical reaction. A laser Doppler vibrometer (LDV) was used to examine the reliability of the EMMA, and the results of this testing are shown in Fig. 15(b). For an applied current of 180 mA, the displacement deviations remained within 4% following 24,000 operating cycles. The deviations increased to approximately 7% when the applied current was increased to 360 mA, which might result from the escalated effect of joule heating. Methods of reducing the joule heating are required if the actuator needs to be operated at high current with good reliability. Fig. 16 illustrates the dynamic testing result of the EMMA. The first resonant frequency is around 1.43 kHz, which can provide a high volume flow rate for operating as a reciprocating micropump. The embedded depth of coil can also be modified without reediting the mask patterns for different resonant frequencies.

5. Discussion

Some of our simulation results indicate that the maximum deformation of the EMMA varied according to various design parameters. For example, the layout of embedded coils on PDMS membrane can influence both electromagnetic force and membrane stiffness. On one hand, the closer the coil position is to the edge of permanent magnet, the larger the electromagnetic force that can be obtained. On the other hand, the effective stiffness is larger if the coil is placed further from the center of membrane. In designing the EMMA, the above guideline as well as those described in Section 2.1 can be adopted to generate preliminary design values. However, obtaining general or optimal design parameters is still difficult owing to numerous other influences, including membrane diameter, coil pitch, and number of coil turns. Consequently, the optimal design can only be determined on a case-by-case basis.

While operating the EMMA, numerous cracks on the PDMS membrane could be observed when applying a current exceeding 500 mA. This phenomenon results mainly from the joule heating effect of the coil. Besides impacting stability, this phenomenon may damage the membrane device. It is difficult to completely eliminate the influence of this phenomenon since both the electromagnetic force and joule heating depend on the same current. One way to reduce the effect of this phenomenon is to avoid operating the EMMA at high current, while another way is to introduce a heat-dissipation path to remove the generated heat.

6. Conclusion

This study reports the implementation of a novel electromagnetic EMMA with a semi-embedded coil. A batch process for fabricating thin PDMS membrane embedded with a planar coil, which is the essential part of EMMA, is proposed and demonstrated. An advanced EMMA, which incorporates a semi-embedded coil, is also proposed. The proposed design possesses several advantages, including improved fabrication yield, adjustable stiffness, and reliability. The characterization for PDMS membrane, including thin film preparation, resistance to etching, adhesion improvement, and gas-permeation property are also elaborated. Experimental results demonstrate that the maximum deflection can reach 55 μm, equivalent to a pumping volume exceeding 2 μl. The test for short-term stability reveals that no obvious deflection deviation is observable in a 30 min test. In a long-term periodical test, the displacement deviations remained within 7% after 24,000 operating cycles.

The proposed design fulfills the requirements of large flexibility, good controllability, system compactness and batch-process capability. Combining the EMMA with a valve-control microfluidic chip controls microflow simply and effectively, enabling portable biomedical analysis apparatus to be realized.

Acknowledgements

The authors would like to thank Nation Science Council, Taiwan, for supporting this research under grant number NSC-95-2221-E-492-005. The authors would also like to acknowledge Mr. Sheng-Yi Hsiao and Mr. Wen-Chih Chen in NTHU, Mr. Yu-Hsin Lin and Dr. Da-Ren Liu in ITRC, for their valuable assistances on this work.

References

[1] C.H. Ahn, J.-W. Choi, G. Beaucage, J.H. Nevin, J.-B. Lee, A. Puntambekar, J.Y. Lee, Disposable smart lab on a chip for point-of-care clinical diagnostics, Proc. IEEE 92 (1) (2004) 154–173.

[2] D.J. Laser, J.G. Santiago, A review of micropumps, J. Micromech. Microeng. 14 (6) (2004) R35–R64.

[3] M. Koch, A.G.R. Evans, A. Brunnschweiler, The dynamic micropump driven with screen printed PZT actuator, J. Micromech. Microeng. 8 (2) (1998) 119–122.

[4] B. Tarik, B. Alain, P.G. Jean, Design and simulation of an electrostatic micropump for drug-delivery applications, J. Micromech. Microeng. 7 (3) (1997) 186–188.

[5] A. Wego, L. Pagel, A self-filling micropump based on PCB technology, Sens. Actuators A 88 (3) (2001) 220–226.

[6] C.R. Neagu, J.G.E. Gardeniers, M. Elwenspoek, J.J. Kelly, An electrochemical microactuator: principle and first results, J. Microelectromech. Syst. 5 (1) (1996) 2–9.

[7] M. Kohl, K.D. Skrobanek, S. Miyazaki, Development of stress-optimized shape memory microvalves, Sens. Actuators A 72 (3) (1999) 243–250.

[8] M. Khoo, C. Liu, Micro magnetic silicone elastomer membrane actuator, Sens. Actuators A 89 (3) (2001) 259–266.

[9] S. Bohm, W. Olthuis, P. Bergveld, A plastic micropump constructed with conventional techniques and materials, Sens. Actuators A 77 (3) (2001) 223–228.

[10] O.C. Jeong, S.S. Yang, Fabrication and test of a thermopneumatic micropump with a corrugated p+ diaphragm, Sens. Actuators A 83 (1–3) (2000) 249–255.

[11] M. Eiji, M. Takayuki, Fabrication of TiNi shape memory micropump, Sens. Actuators A 88 (3) (2001) 256–262.

[12] X. Yang, Y.-C. Tai, C.-M. Ho, Micro bellow actuators, in: Proceedings of Transducers '97: Dig. Tech. Papers, International Conference on Solid-State Sensors and Actuators, Chicago, 16–19 June 1997, pp. 45–48.

[13] K.H. Kim, H.J. Yoon, O.C. Jeong, S.S. Yang, Fabrication and test of a micro electromagnetic actuator, Sens. Actuators A 117 (1) (2005) 8–16.

[14] C.J. Van Mullem, K.J. Gabriel, H. Fujita, Large deflection performance of surface micromachined corrugated diaphragms, in: Proceedings of Transducers '91: Dig. Tech. Papers, International Conference on Solid-State Sensors and Actuators, San Francisco, 24–27 June 1991, pp. 1014–1017.

[15] W.Y. Sim, H.J. Yoon, O.C. Jeong, S.S. Yang, A phase-change type micropump with aluminum flap valves, J. Micromech. Microeng. 13 (2) (2003) 286–294.

[16] C. Yamahata, F. Lacharme, J. Matter, S. Schnydrig, Y. Burri, M.A.M. Gijs, Electromagnetically actuated ball valve micropumps, in: Proceedings of Transducers '05: Dig. Tech. Papers, International Conference on Solid-State Sensors and Actuators, Seoul, Korea, 5–9 June 2005, pp. 192–196.

[17] H.-L. Yin, J. Hsieh, H.-H. Hsu, A novel elastomer membrane micropump with embedded coils for off-chip pumping applications, in: Proceedings of MEMS 2006: Dig. Tech. Papers, International Conference on Micro Electro Mechanical Systems, Istanbul, Turkey, 22–26 January 2006, pp. 770–773.

[18] Q. Ramadan, V. Samper, D. Poenar, C. Yu, On-chip micro-electromagnets for magnetic-based bio-molecules separation, J. Magn. Magn. Mater. 281 (2004) 150–172.

[19] D.K. Cheng, Field and Wave Electromagnetics 2/e, Addison Wesley Longman, Ch.6.

[20] A. Meckes, J. Behrens, W. Benecke, Electromagnetically driven microvalve fabricated in silicon, in: Proceedings of Transducers '97: Dig. Tech. Papers, International Conference on Solid-State Sensors and Actuators, Chicago, 16–19 June 1997, pp.821–824.

[21] A.C. Ugural, Stresses in Plates And Shells, WCB McGraw-Hill, 1999, Ch. 4.

[22] M. Richter, R. Linnemann, P. Woias, Robust design of gas and liquid micropumps, Sens. Actuators A 68 (3) (1998) 480–486.

[23] Y.-H. Lin, H.-L. Yin, Y.-Y. Hsu, Y.-C. Hu, H.-Y Chou, T.-H. Yang, SCREAM for multi-level moveable structures by inductively coupled plasma process, in: Proceedings of IMECE 2002: Dig. Tech. Papers, ASME International Mechanical Engineering Congress and Exposition, New Orleans, Louisiana 17–22 November 2002, IMECE2002-33382.

Biographies

Hung-Lin Yin was born in Tainan, Taiwan, in 1977. He received his MS degree in power mechanical engineering from National Tsing Hua University in 2001. In 2001, he worked as an assistant researcher at Instrument Technology Research Center, Taiwan. His research interests include MEMS with emphasis on micro fabrication technologies, LIGA-like process, microactuators, the characterization of the mechanical properties of microstructures, and electron beam lithography.

Yu-Che Huang was born in Yilan, Taiwan, in 1980. He received his Master degree from the Aerospace and System Engineering Department of Feng Chia University in 2004. Currently he is studying for the PhD degree in Power Mechanical Engineering Department, National Tsing Hua University, Taiwan. His major research interests include LIGA-Like fabrication process, magnetic actuators, microfluidic chip, and finite element analysis.

Weileun Fang was born in Taipei, Taiwan, in 1962. He received his PhD degree from Carnegie Mellon University in 1995. His doctoral research focused on the determining of the mechanical properties of thin films using micromachined structures. In 1995, he worked as a postdoctoral research at Synchrotron Radiation Research Center, Taiwan. He joined the Power Mechanical Engineering Department at the National Tsing Hua University (Taiwan) in 1996, where he is now a Professor as well as a faculty of MEMS Institute. From June to September 1999, he was with Prof. Y.-C. Tai at California Inst. Tech. as a visiting associate. He has established a MEMS testing and characterization lab. His research interests include MEMS with emphasis on micro fabrication/packaging technologies, micro optical systems, microactuators, and the characterization of the mechanical properties of thin films.

Jerwei Hsieh was born in Taipei, Taiwan, in 1973. He received his Master and PhD degrees from Power Mechanical Engineering at National Tsing-Hua University in 1998 and 2002, respectively. Since 2002, he worked as an associate researcher at Instrument Technology Research Center, National Applied Research Laboratories, Taiwan. His research interests include MEMS with emphasis on micro transducers, optical microsystems, microfluidic devices for bio application, and process integration to various micromachining technologies.